

# Harvesting Human Being Energy to Charge Smartphone

Elaf J. Majeed<sup>1</sup>, Amani J. Majeed<sup>2\*</sup>

<sup>1</sup>University of Basrah, College of Engineering, Electrical Engineering Department, Iraq

<sup>2</sup>University of Basrah, College of Engineering, Petroleum Engineering Department, Iraq

Received 21 Nov 2021

Accepted 17 Apr 2022

## Abstract

Rapid development has occurred recently in the use of thermoelectric generators (TEGs), as they have been applied in numerous fields. Although TEGs can harvest the body's energy, the output voltages they yield are extremely small (a few hundred mV). Accordingly, the objective of this paper is to study the possibility of enlarging a voltage generated by the TEG to a level where it can be used.

In this paper, we provide a comprehensive simulation of the performance of TEGs system that harvests human energy by using one topology of the conversion circuit, the DC/DC step-up converter, that raises the external voltage so that portable mobile devices can be charged. In the proposed system ten pieces of the TEGs have been used, every system contains 35 TEG couples connected serially by legs. The methodology of the current study focuses on using the finite element method (FEM) to simulate the TEG system, where we used ANSYS Workbench software platform (Professional Version 18.1). Moreover, MATLAB and PSPICE Simulink have been used to simulate the energy conversion circuit. The outcomes of this study can be summarized in the following points: 1) the total voltage obtained from the ten pieces of the TEG system is about (2.165V). 2) Using the boost DC/DC converter system help to enlarge the total voltage of TEG to 5 Volt. 3) There is no signifying effect for the different shapes of TEG legs, where a comparison was made between two different shapes of TEG legs, one is rectangular and the other is equivalent cylindrical. 4) The results of TEG were also compared with the results of previous work, and a good agreement has been attained. 5) MATLAB - PSPICE simulation programs were used to design and implement the DC-to-DC boost converter circuit, and the results showed the output response of the overall system being in line with the study objectives.

© 2022 Jordan Journal of Mechanical and Industrial Engineering. All rights reserved

**Keywords:** Thermoelectric generator, Human body temperature, DC/DC boost converter, Seebeck effect.

## Nomenclature

$A$	Area [m <sup>2</sup> ]	$V$	Voltage [V]
$c$	Heat capacity [J kg <sup>-1</sup> K <sup>-1</sup> ]	$V_d$	Forward voltage drop [V]
$C$	Filter capacitance [F]	$V_L$	Inductor voltage [V]
$D$	The duty cycle [-]	Greek letters	
$E$	Electric field [V m <sup>-1</sup> ]	$\Delta$	Difference
$F_s$	Switching frequency [Hz]	$\eta$	Conversion efficiency
$I_L$	Inductor current [A]	$\kappa$	Thermal conductivity [W m <sup>-1</sup> K <sup>-1</sup> ]
$J$	Electric current flux [A m <sup>-2</sup> ]	$\rho$	Density [kg m <sup>-3</sup> ]
$k$	Heat transfer coefficient [W m <sup>-2</sup> K <sup>-1</sup> ]	$\rho_c$	Charge density [C m <sup>-3</sup> ]
$L$	Inductance [Henry]	$\rho_e$	Electrical resistivity [ $\Omega$ m]
$P$	Electric power [W]	$\sigma$	Electrical conductivity [S m]
$P'$	Peltier coefficient [-]	$\tau$	Time period [s]
$Q$	Heat power [W]	Abbreviations	
$Q'$	Density of Joule heating energy [W m <sup>-3</sup> ]	TEG	Thermoelectric generator
$q''$	Heat flux [W m <sup>-2</sup> ]	DC	Direct current
$R$	Electrical resistance [ $\Omega$ ]	CCM	Continuous current mode
$R_{DS}$	Drain source ON-state resistance [ $\Omega$ ]		
$R_L$	Inductor resistance [ $\Omega$ ]		
$S$	Seebeck coefficient [V K <sup>-1</sup> ]		
$T$	Absolute temperature [K]		
$T_s$	Switching cycle [s]		
$T_{ON}$	ON state time [s]		
$T_{OFF}$	OFF state time [s]		
$t$	Time [s]		

## 1. Introduction

Globally, electric power generation is shifting to more environment-friendly methods, since the use of conventional sources of energy causes more environmental issues, including global warming, greenhouse gases, and air pollution. This makes the use of renewable energy resources crucial. Solar energy has been used in many applications, including electric power generation and in water

\* Corresponding author e-mail: amani.majeed@uobasrah.edu.iq.

desalination processes, so a great deal of research has focused on developing it as a clean energy resource [1]–[5]. Moreover, wind energy has been growing rapidly as one of the cleanest sources of energy in recent years [6]–[10]. However, a new renewable energy sources must be found to counteract fossil energy's depletion by utilizing existing energy resources and seeking new ways of utilizing them. One of the latest renewable energy sources is thermoelectric generators (TEG) [11].

Science has strongly focused on the use of thermoelectric generators. Nevertheless, a difference in temperature between two semiconductor materials can reveal differences in voltage across these materials, according to Seebeck in 1822 [12]. TEGs have no moving parts and can generate electrical energy from geothermal and solar energy reliably and sustainably [13], [14]. Furthermore, it can be used at nuclear power plants for micro-power generation in the absence of severe accidents to ensure that sensors or indicators are functioning properly [15]. Mateu et al., 2007, used thermoelectric generator modules (TEGs) to harvest the body's energy and supply it to a wireless sensing module. Their hypothesis was that the TEG heat source comes from the human body and the ambient temperature can be represented by the TEG sink source [16]. Moreover, TEGs have been used for several decades to power space vehicles [17], [18]. In 2013, Hadjistassou et al., proposed a new design methodology based on a computational and analytical analysis, where a segmented thermoelectric generator is proposed having a heat source temperature of 622.8 K and a heat sink temperature of 298.2 K [19]. The study resulted in increased analytical accuracy. Considering its time-efficient framework, the hybrid computational-analytical modeling approach achieves a very good level of accuracy [19]. Elsheikh H. Mohamed, et al. (2014) introduced an in-depth review of thermoelectric materials and outlined parameters that contribute to the figure of merit thermoelectric efficiency (ZT). Furthermore, a discussion of the possibilities for optimizing thermoelectric materials was also discussed [20]. Kossyvakis D. N. et al., 2016 examined the performance of a tandem PV-TEG hybrid by using both poly-Si and dye-sensitized solar cells. Different thermoelectric devices with different thermoelement geometries were tested to determine their effect on performance. Additionally, the results of the experimental process have been utilized in order to evaluate the performance of the system under real-world operating conditions. According to the results of the analysis conducted, when actual operating conditions are taken into account, TEGs with shorter thermoelements result in increased power output levels [21]. In 2018, Wang et al. developed a wearable TEG that can power electronic devices (such as a miniaturized accelerometer) by harnessing the energy of the human body. They used 52 pairs of N-type and P-type legs, which were cubic-shaped and made from powder materials derived from Bi<sub>2</sub>Te<sub>3</sub>. They demonstrated that their novel TEG generated 37.2 mV with only a 50 K temperature change for open circuit systems [22].

Moreover by using TEG, Proto et al., in 2018, analyzed the results of measuring the thermal energy harvested from human arms and legs. Four large areas from the skin (Biceps brachii, Flexor carpi radialis, Gracilis, and Gastrocnemius muscle) have been chosen as placement of TEG. Furthermore, users can perform daily activities such as walking, riding a bike, jogging, and sitting. The authors

concluded that the power generated took the range of (5–50  $\mu$ W) and indicated that legs could be used as a placement for TEG due to the variety of biomechanical work generated by the gastrocnemius muscle [23]. In addition, TEG is used to recover waste heat, where Khalil and Hassan presented a 3D study in 2020 of how to enhance lost heat recovery by using TEG in chimneys via heat spreaders. In their study, the authors investigated how different sizes of heat spreaders affected the TEGs' performance that were used to recover heat from chimneys. As a result, the heat spreaders proved to be an effective way to recover waste heat from chimneys via TEGs while saving the initial fixed costs of the system. Where, TEGs' total power increased by 42% when 140 mm heat spreaders were used [24]. Furthermore, Kanagaraj N. 2021, investigated the performance and the design of a hybrid photovoltaic–thermoelectric generator system using fractional-order fuzzy logic controllers-based maximum power point tracking. Where he studied the performance of the proposed maximum power point tracking (MPPT) technique under various thermal and electrical operating conditions by using a MATLAB simulation. According to the author results, the PV and TEG combined system provides higher energy efficiency than the PV module alone [25]. Al-Qadami et al. in 2022, presented a systematic review of the potentials of harvesting thermal energy from asphalt pavements and assesses the progress being made towards developing these technologies through bibliometric analysis. Moreover, they discussed the principles and basics of three main types of thermal energy harvesting technologies. Furthermore, they also described the system's configurations, efficiency, and materials [26].

It is noteworthy that the TEGs are small, lightweight, reliable energy converters since there are no mechanical parts to cause vibration or noise [27]. Despite TEG advantages, their applications are limited because of the high cost [28]. Therefore, in recent years many kinds of research have focused on TEG materials and geometry in order to get the optimum performance at low cost [29]–[32].

The previous studies focused exclusively on using energy directly from thermoelectric generators, which restricted their work to applications that required a low voltage, or used large numbers of TEGs to increase the output voltage level, which increased the overall cost of the system. Therefore, in this study, we intend to use only a few TEGs in order to achieve a relatively high voltage that is suitable for portable devices, such as mobile phones. Besides, an integrated simulation is conducted for a TEG system, as well as a boost DC/DC converter circuit for raising the TEG output voltage. The effect of different shapes on the output voltage was also examined by simulating two different TEG leg shapes, one with a rectangular shape and the other with a cylindrical shape.

## 2. Methodology

According to Fig. 1, the temperature of the human body is converted by the TEG into an electrical voltage, and this voltage is used as input for the DC/DC boost converter system to get an appropriate voltage which will be used for charging purpose. Therefore, the methodology contains two parts; the TEG part and the DC/DC boost converter system part.

2.1. Thermoelectric Generator (TEG)

The thermoelectric generator uses the difference in temperature between two sides to generate power. Therefore, one side needs to work as a heat source, while the other works as a sink source. The difference in temperature makes the electrons vibrate more intensely on the side with higher temperatures, which makes them move more slowly on the side with lower temperatures. As a result of this movement, the current appears, which can then be exploited as electrical energy. The TEG material used in this study is based on bismuth telluride (Bi2Te3). However, it consists of a ceramic plate (to enhance thermal conductivity), electrode solder material (to reduce thermal stress), and a pair of semiconductor legs; P-type and N-type, as shown in Fig. 2.

The behavior of the TEG materials are governed by the heat transfer equation coupled with the density continuity equation as follows [33], [34];

In thermoelectric analysis, the heat flow equation is:

$$\rho c \frac{\partial T}{\partial t} + \nabla \cdot q'' = Q' \tag{1}$$

Where; T represents the temperature; t is the time; c represents the heat capacity; q'' represents a heat flux, and Q' is the Joule heating energy.

The continuity equation for electric charge is;

$$\nabla \cdot J = \frac{\partial \rho_c}{\partial t} \tag{2}$$

Where; J represents the flux of the electric current produced by the coupled Seebeck and Joule effects, and  $\rho_c$  denotes to charge density.

The Joule heating energy and the heat flux are expressed as

$$q'' = -K \nabla T + P' J \tag{3}$$

$$Q' = J \cdot E \tag{4}$$

Where;

$$P' = ST \tag{5}$$

$$J = -\sigma \nabla V - \sigma S \nabla T \tag{6}$$

By substituting Eq. (3-6) in Eq. (1) and Eq. (2), the governing equations will be written as follows:

$$\rho c \frac{\partial T}{\partial t} + \nabla \cdot (-K \nabla T + \alpha T (-\sigma \nabla V - \sigma S \nabla T)) = (-\sigma \nabla V - \sigma S \nabla T) (-\nabla V) \tag{7}$$

$$-\sigma (\nabla^2 V + \alpha \nabla^2 T) = \frac{\partial \rho}{\partial t} \tag{8}$$

In Fig. 3, the geometric entries and dimensions have been explained for one piece of the studying system of rectangular and equivalent cylindrical TEG legs. Ten pieces of the TEG system have been used as demonstrated in Fig. 4. Every system contains 35 TEG couples connected serially by legs. The steady-state case has been assumed, and the human temperature represents a heat source for the TEG while the ambient temperature is used as a cold part of TEG.

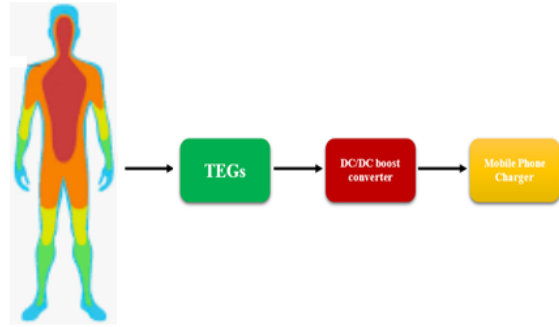


Figure 1. Block diagrams of the system

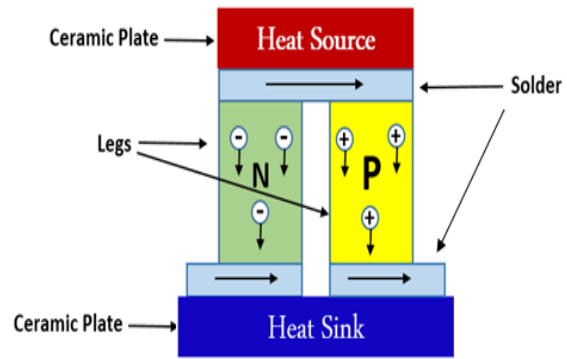


Figure 2. Thermoelectric Generator

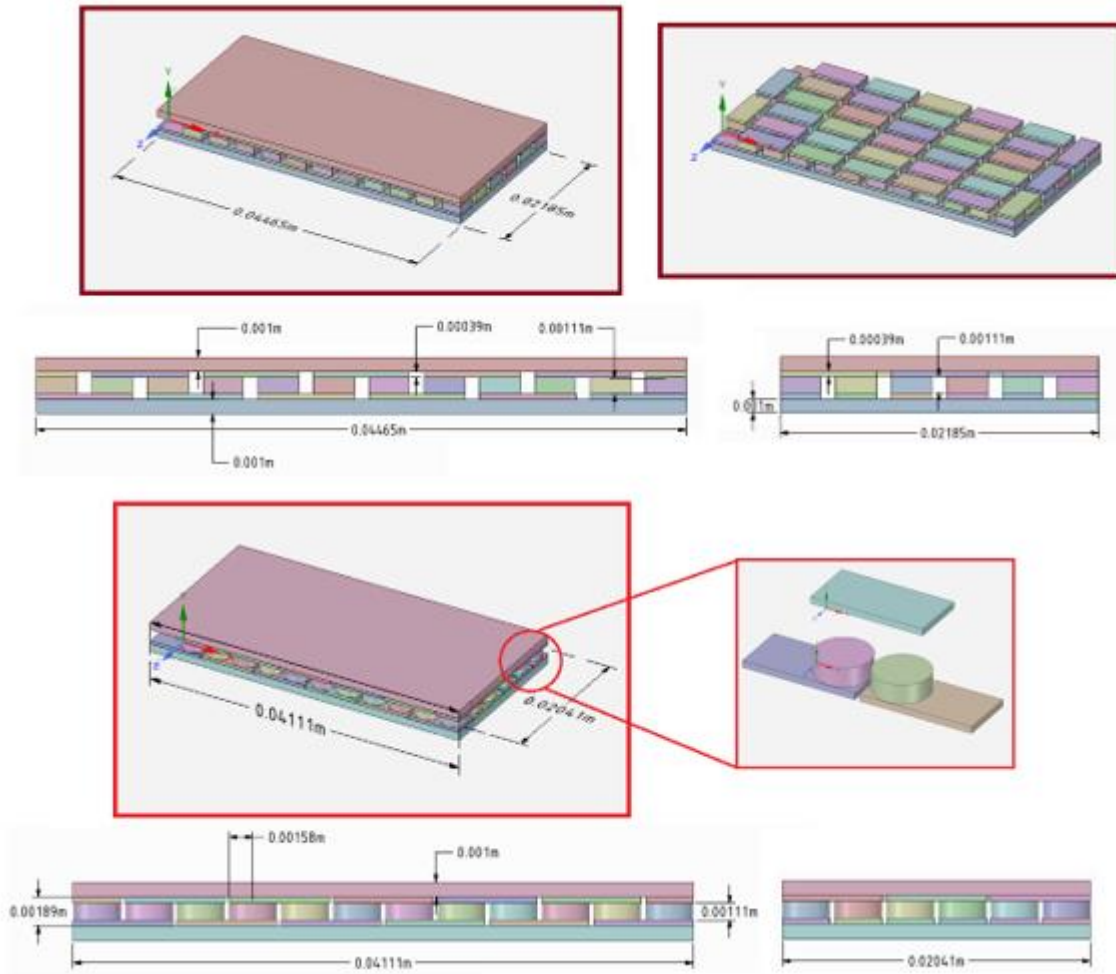


Figure 3. TEG geometry: (a) One piece of TEG with rectangular legs, (b) One piece of TEG with equivalent cylindrical legs

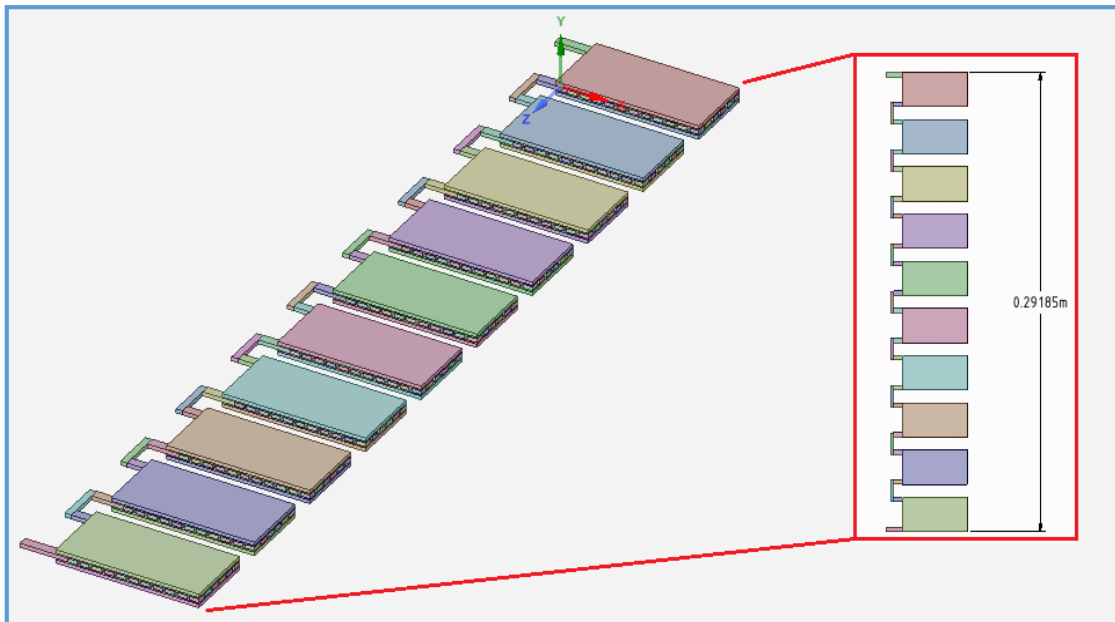


Figure 4. Ten pieces of TEG connected serially

Table 1 lists the parameters of the N-Type and P-Type components of the TEG part that were simulated with the ANSYS software package. Further, the ceramic plate has a thermal conductivity of  $36.5 \text{ W m}^{-1} \text{ K}^{-1}$ , while the resistivity and thermal conductivity of the solder layers are  $1.68 \times 10^{-8} \text{ } \Omega \text{ m}$  and  $390 \text{ W m}^{-1} \text{ K}^{-1}$ , respectively.

**Table 1.** The parameters of the TEG materials used in this study [35].

Components	Seebeck coefficient [V K <sup>-1</sup> ]	Resistivity [ $\Omega \text{ m}$ ]	Thermal conductivity [ $\text{W m}^{-1} \text{ K}^{-1}$ ]
P-Type	0.0002	$8.8 \times 10^{-6}$	1.55
N-Type	-0.0002	$1 \times 10^{-5}$	1.605

**2.2. DC-to-DC Boost converter circuit**

DC-DC power stage converters can be used in portable devices to generate the desired DC level. They can also be used to reduce ripples, and carry out a variety of other functions, such as modifying the voltage level (up or down steps), and regulating voltage.

Boost converter circuits provide greater output voltages than input voltages due to the equipment arrangement. By using the mentioned converter, the TEG output voltage increased to a much more suitable voltage for phone charging. The schematic diagram of the DC/DC asynchronous boost converter is shown in Fig. 5.

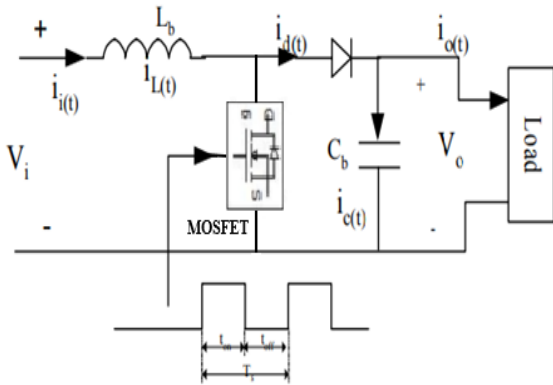


**Figure 5.** Asynchronous step-up DC/DC Converter Circuit Schematic.

Based on the continuous conduction mode (CCM) of the converter circuit, the inductor current flows continuously during the whole switching period. As a ramification, the boost power stage assumes two states per switching cycle. The ON state where the switch Q is on while diode D is blocked. During this stage, the current through the inductor L increase linearly and energy is stored in the inductor. The capacitor C supplies energy to the load R. The OFF state starts when the switch is off and the diode becomes conductive, the energy stored in the inductor L is returned to the capacitor and the load R. As shown in Fig. 6.

The duration of the ON stat  $T_{on}$  is given by  $DT_s$ , where D is the duty cycle curb by the control circuit, came across as a ratio of the switch ON time to the time of one complete switching cycle,  $T_s$ . The duration of the OFF state is  $T_{off}$ , and for continuous conduction mode, is equal to  $(1 - D)T_s$  as there are only two states per switching cycle. These times are shown along with the waveforms in Fig.7.

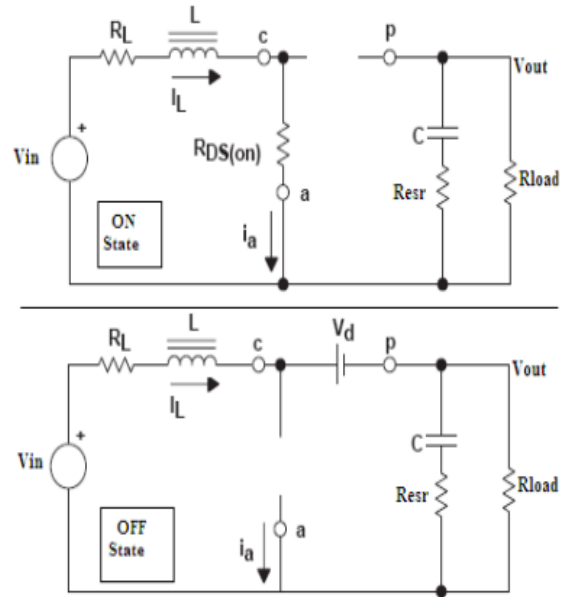


**Figure 6.** Boost Power Stage States [36]

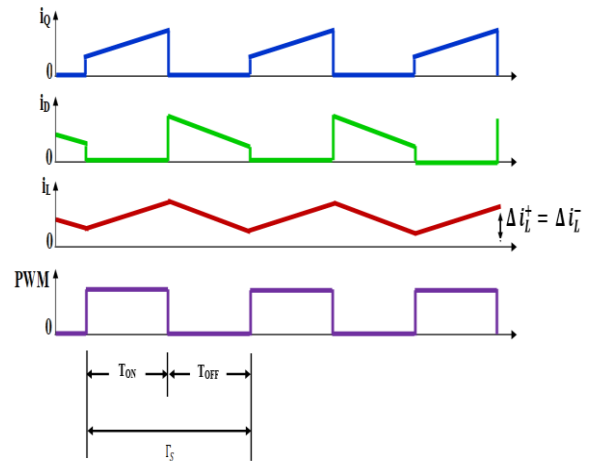


**Figure 7.** Waveforms of current and voltage in continuous inductor current mode (CCM)

Referring to Fig.6, Fig.7 and [36], the inductor-current increase is calculated by using the familiar relationship, when the circuit is ON;

$$V_L = L \times \frac{di_L}{dt} \rightarrow \Delta I_L = \frac{V_L}{L} \times \Delta T \tag{9}$$

Therefore, the inductor current increases during the on state is:

$$\Delta I_L^{(+)} = \frac{V_{in} - (R_{DS} + R_L)I_L}{L} \times T_{ON} \tag{10}$$

Where the  $\Delta I_L^{(+)}$  represents the inductor ripple current. The output capacitor C provides all the output load current during this period.

Conversely, inductor current decreases during the OFF state as follows:

$$\Delta I_L^{(-)} = \frac{(V_{out} + V_d + I_L \times R_L) - V_{in}}{L} \times T_{OFF} \tag{11}$$

Where the  $\Delta I_L^{(-)}$  represents the inductor ripple current also.

Under steady-state conditions, the current increase during on-time  $\Delta I_L^{(+)}$ , and the current decrease during off-time,  $\Delta I_L^{(-)}$ , equalize. Alternatively, the inductor current would otherwise have a net increase or decrease from cycle to cycle, which would not constitute steady state.

Thus, by equalizing Eq. (10) and Eq. (11), the continuous conduction mode boost voltage conversion relationship can be obtained:

$$V_{out} = (V_{in} - I_L \times R_L) \times \left(1 + \frac{T_{ON}}{T_{OFF}}\right) - V_d - V_{DS} \times \left(\frac{T_{ON}}{T_{OFF}}\right) \quad (12)$$

Let  $T_s = T_{ON} + T_{OFF}$ ,  $D = \left(\frac{T_{ON}}{T_s}\right)$ , and  $(1 - D) = \frac{T_{OFF}}{T_s}$ , then the steady-state equation for  $V_{out}$  is:

$$V_{out} = \frac{V_{in} - I_L \times R_L}{1 - D} - V_d - V_{DS} \times \frac{D}{1 - D} \quad (13)$$

Since the  $R_L$ ,  $V_d$ , and  $V_{DS}$  are insignificant enough to ignore, then Eq. (13) becomes:

$$V_{out} = \frac{V_{in}}{1 - D} \quad (14)$$

The boost inductance is defined as [37], [38]:

$$L = \frac{RD(1-D)}{2F_s} \quad (15)$$

Moreover, the switching frequency,  $F_s$  is presumed to be (25000 Hz).

For the boost output filter capacitor, Eq. 16 gives the required capacitance value (C) as a function of ripple voltage ( $\Delta V_o$ ), the duty cycle (D), the switching frequency  $F_s$ , and the output voltage [37], [38], and [39]:

$$C \geq \frac{V_o D}{F_s \Delta V_o R} \quad (16)$$

The output voltage ripple is assumed to be 1%.

### 3. Results and Discussion

#### 3.1. TEG simulation results

Ten pieces of the TEG system have been used. Each system consists of 35 TEGs connected serially by legs. Due to the difference in temperature between the cold and hot TEG legs sides and since these legs are serially connected, the electric voltage will be generated (which is already the Seebeck effect phenomenon). Fig. 8, shows the 3D voltage distribution for one piece of TEG when the TEG legs have a rectangular form.

Also, Fig. 9, shows the 3D electric voltage distribution but when the TEG legs have an equivalent cylindrical shape. Fig. 9-b, gives more visualization about the entries of the system, where the shape of TEG legs has been explicitly exposed.

Fig. 10 and Fig. 11 show the 3D TEGs temperature distribution for rectangular and cylindrical TEG legs form, respectively. The hot side of the TEG is represented by human body temperature (which is 37.8 C), while the cold TEG side is the ambient temperature. It is obvious that the difference is very little in the value of the electric voltage coming out of the two mentioned TEG shapes, where the percentage of the difference is about (0.2%). Moreover, the conformity of the results of the TEG part for the current work with the published work [35], can be seen in Fig. 12, which confirms the accuracy of the results obtained in this study, where a human body temperature of 37.8 degrees Celsius represents the hot side of the TEG, whereas the ambient temperature represents the cold side.

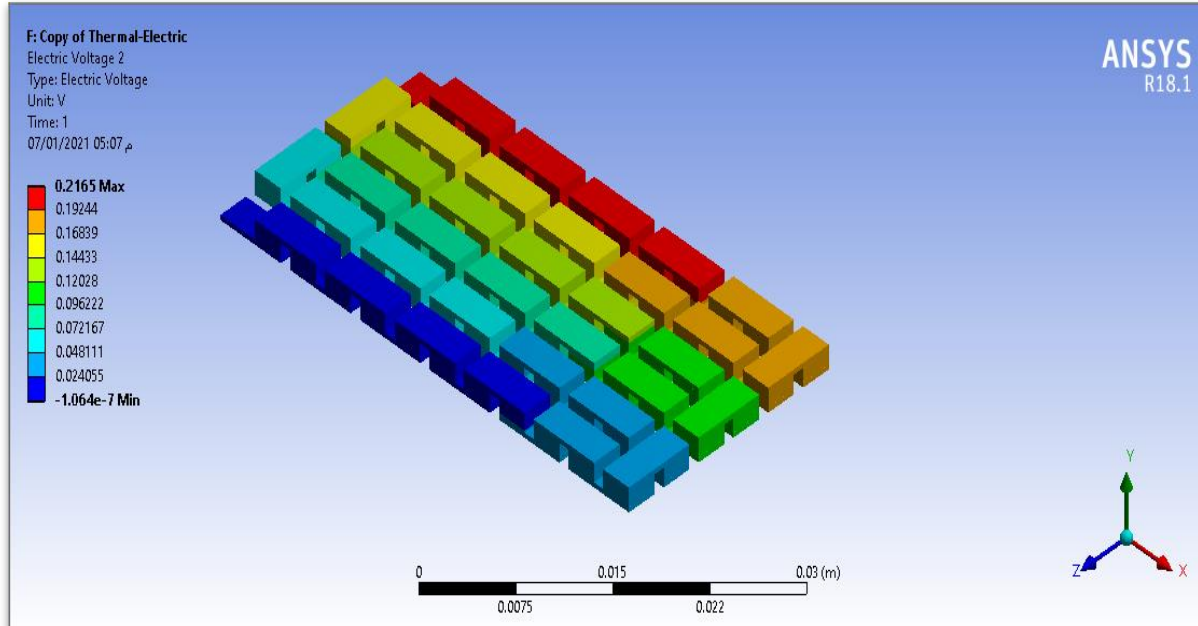


Figure 8. Volt distribution on one piece that contains 35 TEG couples with rectangular TEG legs shape.

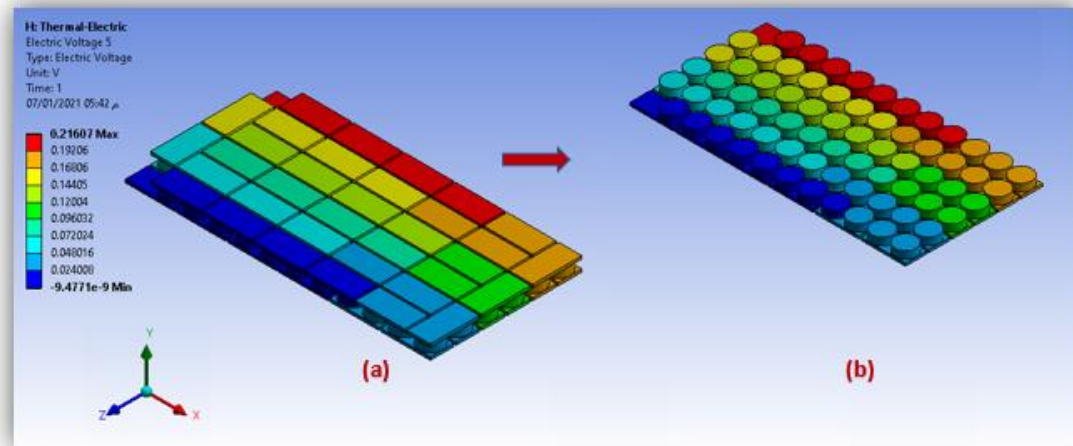


Figure 9. Volt distribution on one piece that contains 35 TEG couples with equivalent cylindrical TEG legs shape.

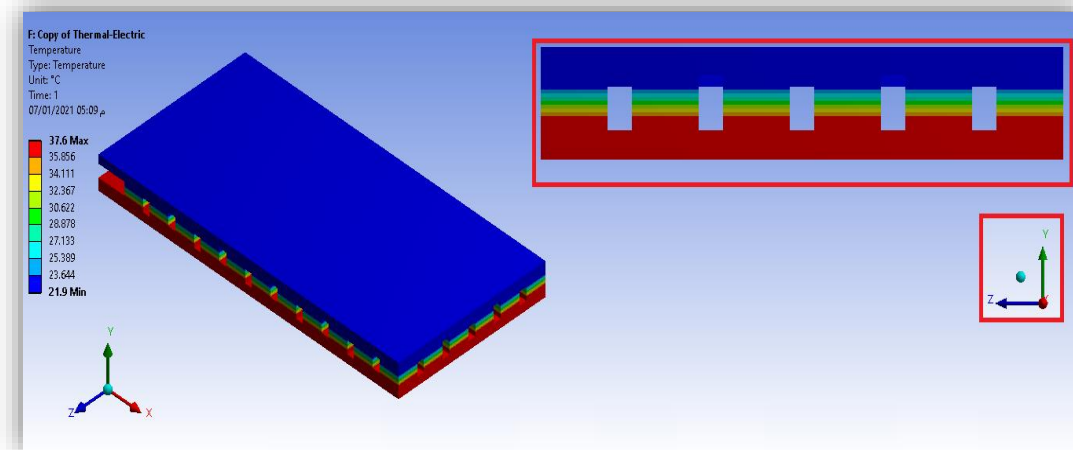


Figure 10. Temperature distribution on one piece that contains 35 TEG couples with rectangular TEG legs shape.

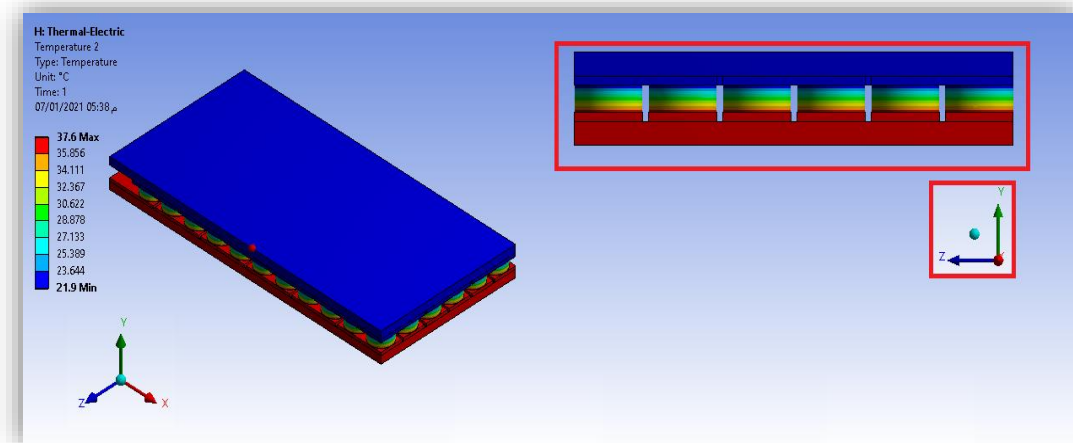


Figure 11. Temperature distribution on one piece that contains 35 TEG couples with equivalent cylindrical TEG legs shape.

3.2. Boost converter Simulation Results:

The boost converter, an asynchronous circuit, is modeled in Matlab/Simulink as shown in Fig. 13. The voltage input to this model comes from TEG systems (which is 2.165 V), with a switching frequency 25 kHz.

Fig. 14, reveals the output voltage of the converter concerning time obtained from Matlab simulation, which is (5V). While Fig. 15 shows the output current, which is 3000mA. The duty cycle is 0.567 for an operating frequency of 25 kHz.

The circuit diagram used for PSPICE / Simulink of the step-up converter is shown in Fig. 16. The purpose of this circuit is to measure output voltage across the resistor R1, Moreover, Fig. 17 shows the output voltage across R1 which becomes stable after sometime, and remains at 5 V.

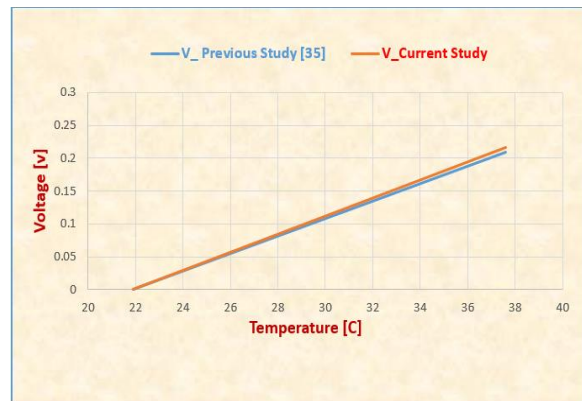


Figure 12. The output electrical voltage vs. temperature.

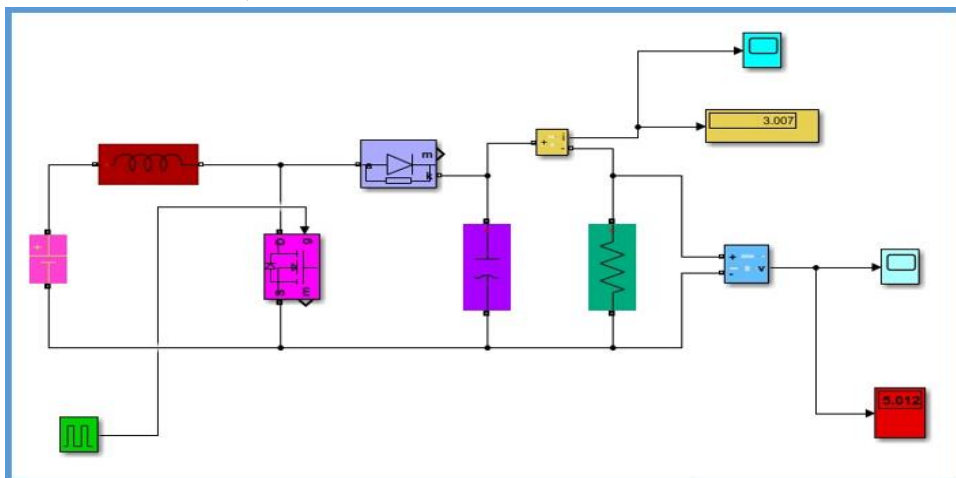


Figure 13. Circuit Diagram of the Boost DC/DC Converter used in MATLAB

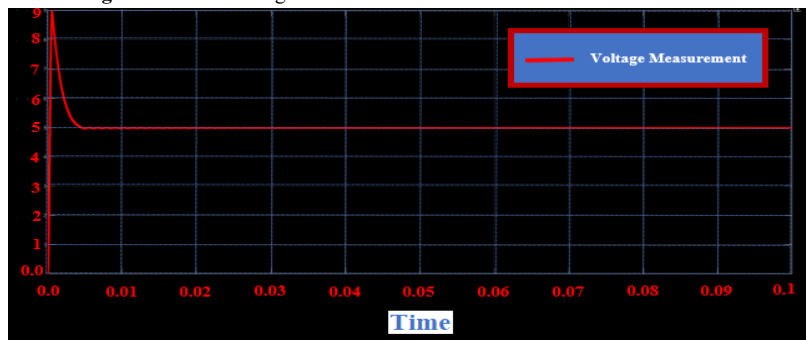


Figure 14. V<sub>o</sub> (Output Voltage) vs time in MATLAB

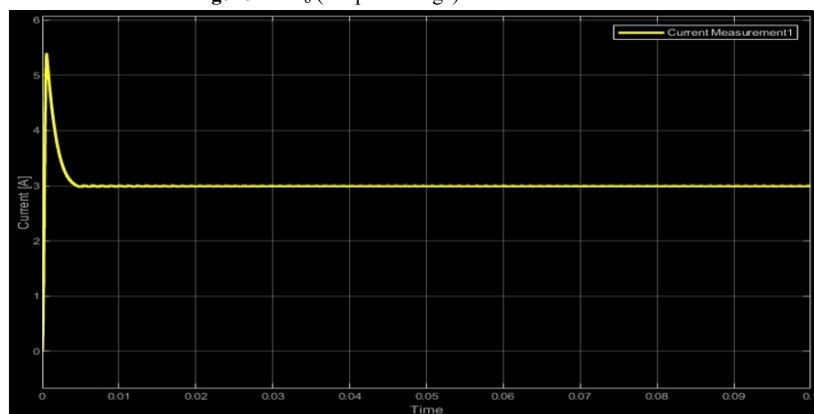


Figure 15. I<sub>o</sub>(output current) vs Time in MATLAB.

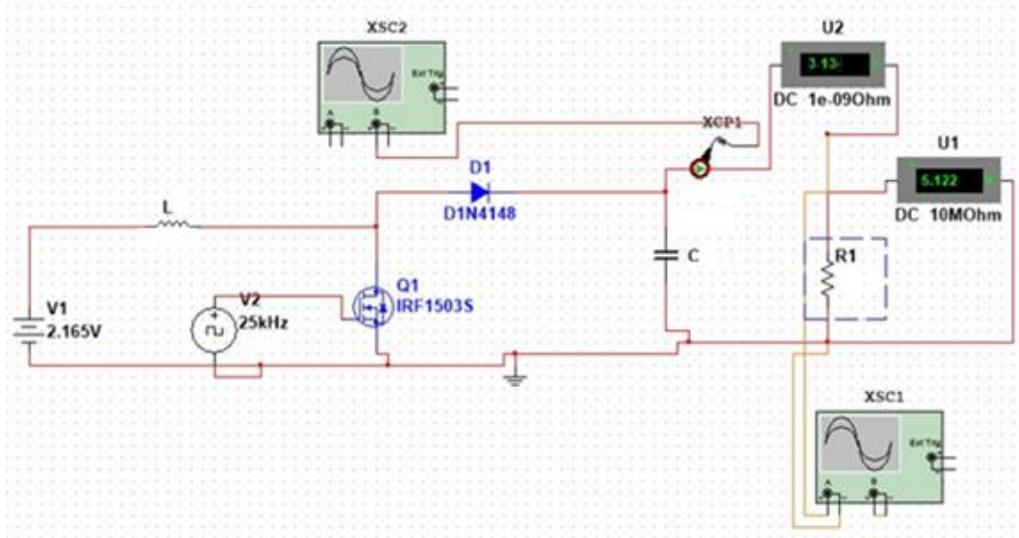


Figure 16. Circuit diagram of boost converter used in P PSPICE

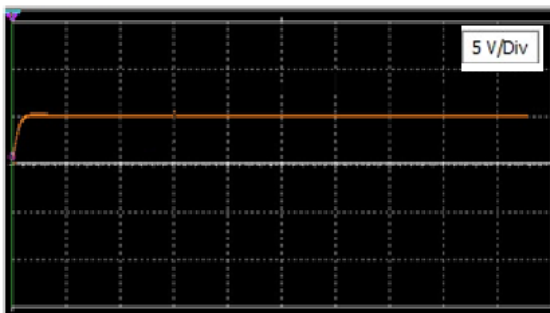


Figure 17.  $V_{out}$  (Output Voltage) vs time in PESPIC

#### 4. Conclusion

A complete modeling and simulation of TEG system with a boost converter circuit was developed. The proposed TEG system consists of ten pieces of the TEGs with a total length of 0.29185 m. Each system that consists of 35 TEG couples connected serially by legs, has been simulated by using the finite element method. There is only a slight difference (0.2%) between the output response of the TEG electric voltage when two different leg shapes are used (the rectangular and equivalent cylindrical ones). In addition, an asynchronous DC to DC boost converter with continuous current mode was established. Simulations were conducted using MATLAB and PSPICE, and corresponding waveforms were obtained. The output voltage across the output capacitor is 5 V with a maximum output ripple of 1%. Based on the results from the simulation programs, we can see that the results obtained are somewhat similar and are also comparable to the desired result from the TEG system and power conversion circuit.

#### References

- [1] Majeed J. Amani, Najim E. Saleh, and Hammadi H. Salaman, "Simulation Solar Electrical Generation Power Plant By Using Parabolic Trough In Basra City," *Al-Qadisiya Journal For Engineering Sciences*, vol. 7, no. 1, pp. 1–11, 2014.
- [2] S. Kiwan, L. Venezia, F. M. Montagnino, F. Paredes, and R. Damsch, "Techno-Economic Analysis of a Concentrated Solar Polygeneration Plant in Jordan," *Jordan Journal of Mechanical and Industrial Engineering*, vol. 12, no.1, pp. 1 – 6, 2018.
- [4] A. J. Majeed and G. J. Mohammed, "Sustainable Energy for Water Desalination System Relative to Basra Climate," *Jordan Journal of Mechanical and Industrial Engineering*, vol.9, no. 2, pp. 129 – 137, 2015.
- [5] M. H. Nehrir et al., "A review of hybrid renewable/alternative energy systems for electric power generation: Configurations, control, and applications," *IEEE Transactions on Sustainable Energy*, vol. 2, no. 4. pp. 392–403, Oct. 2011. doi: 10.1109/TSTE.2011.2157540.
- [6] M. Messaoud, B. Hadi, and D. Aissa, "Sensorless Control System Design of a Small Size Vertical Axis Wind Turbine," *Jordan Journal of Mechanical and Industrial Engineering*, vol.12, no. 2, pp. 93 – 98,2018.
- [7] A. J. M. Al-Hussieni, "A Prognosis of Wind Energy Potential as a Power Generation Source in Basra City, Iraq State," *European Scientific Journal*, vol. 10, no. 36, 2014.
- [8] K. al Bkoo Alrawashdeh, N. S. Gharaibeh, A. A. Alshorman, and M. H. Okour, "Magnus Wind Turbine Effect Vertical Axis Using Rotating Cylinder Blades," *Jordan Journal of Mechanical and Industrial Engineering*, vol.15, no. 2, pp. 233 – 241, 2021.
- [9] E. A. Teshnizi et al., "Comprehensive Energy-Econo-Enviro (3E) Analysis of Grid-Connected Household Scale Wind Turbines in Qatar," *Jordan Journal of Mechanical and Industrial Engineering*, vol.15, no. 2, pp. 215 – 231,2021.
- [10] C. Ghenai, T. Salameh, and I. Janajreh, "Modeling and Simulation of Shrouded Horizontal Axis Wind Turbine Using RANS Method," *Jordan Journal of Mechanical and Industrial Engineering*, vol.11, no. 4, pp. 235 -243,2017.
- [11] C. Cekdin, Z. Nawawi, and M. Faizal, "The usage of thermoelectric generator as a renewable energy source," *Telkommika (Telecommunication Computing Electronics and Control)*, vol. 18, no. 4, pp. 2186–2192, 2020, doi: 10.12928/TELKOMNIKA.V18I4.13072.
- [12] J. T. Seebeck, "Magnetic polarization of metals and minerals," *Abhandlungen der Deutschen Akademie der Wissenschaften zu Berlin*, vol. 265, pp. 1822–1823, 1822.
- [13] C. Suter, Z. R. Jovanovic, and A. Steinfeld, "A 1kWe thermoelectric stack for geothermal power generation - Modeling and geometrical optimization," *Applied Energy*, vol. 99, pp. 379–385, 2012, doi: 10.1016/j.apenergy.2012.05.033.
- [14] A. K. Trinh, I. González, L. Fournier, R. Pelletier, J. C. Sandoval V., and F. J. Lesage, "Solar thermal energy

- conversion to electrical power,” *Applied Thermal Engineering*, vol. 70, no. 1, pp. 675–686, Sep. 2014, doi: 10.1016/j.applthermaleng.2014.05.088.
- [15] L. S. Chen, J. Y. Lee, and I. C. Bang, “Passive Micro Power Generation for Nuclear Safety with Thermoelectric Heat Pipe,” 2013.
- [16] L. Mateu, C. Codrea, N. Lucas, M. Pollak, P. Spies, and F. Iis, “Human Body Energy Harvesting Thermogenerator for Sensing Applications,” 2007, doi: 10.1109/SENSORCOMM.2007.42.
- [17] Rowe D. Michael, *Thermoelectrics Handbook Macro to Nano*, 1st ed. CRC Press, 2005.
- [18] J.-P. Fleurial *et al.*, “2011 THERMOELECTRICS APPLICATIONS WORKSHOP Thermoelectrics: From Space Power Systems to Terrestrial Waste Heat Recovery Applications.”
- [19] C. Hadjistassou, E. Kyriakides, and J. Georgiou, “Designing high efficiency segmented thermoelectric generators,” *Energy Conversion and Management*, vol. 66, pp. 165–172, 2013, doi: 10.1016/j.enconman.2012.07.030.
- [20] M. Hamid Elsheikh *et al.*, “A review on thermoelectric renewable energy: Principle parameters that affect their performance,” *Renewable and Sustainable Energy Reviews*, vol. 30, pp. 337–355, 2014, doi: 10.1016/j.rser.2013.10.027.
- [21] D. N. Kossyvakis, G. D. Voutsinas, and E. v. Hristoforou, “Experimental analysis and performance evaluation of a tandem photovoltaic-thermoelectric hybrid system,” *Energy Conversion and Management*, vol. 117, pp. 490–500, Jun. 2016, doi: 10.1016/j.enconman.2016.03.023.
- [22] Y. Wang, Y. Shi, D. Mei, and Z. Chen, “Wearable thermoelectric generator to harvest body heat for powering a miniaturized accelerometer,” *Applied Energy*, vol. 215, pp. 690–698, Apr. 2018, doi: 10.1016/j.apenergy.2018.02.062.
- [23] A. Proto *et al.*, “Thermal energy harvesting on the bodily surfaces of arms and legs through a wearable thermo-electric generator,” *Sensors (Switzerland)*, vol. 18, no. 6, Jun. 2018, doi: 10.3390/s18061927.
- [24] H. Khalil and H. Hassan, “Enhancement of waste heat recovery from vertical chimney via thermoelectric generators by heat spreader,” *Process Safety and Environmental Protection*, vol. 140, pp. 314–329, Aug. 2020, doi: 10.1016/j.psep.2020.05.023.
- [25] N. Kanagaraj, “Photovoltaic and thermoelectric generator combined hybrid energy system with an enhanced maximum power point tracking technique for higher energy conversion efficiency,” *Sustainability (Switzerland)*, vol. 13, no. 6, Mar. 2021, doi: 10.3390/su13063144.
- [26] E. H. H. Al-Qadami, Z. Mustafa, and M. E. Al-Atroush, “Evaluation of the Pavement Geothermal Energy Harvesting Technologies towards Sustainability and Renewable Energy,” *Energies*, vol. 15, no. 3, MDPI, Feb. 01, 2022, doi: 10.3390/en15031201.
- [27] D. Champier, “Thermoelectric generators: A review of applications,” *Energy Conversion and Management*, vol. 140, Elsevier Ltd, pp. 167–181, 2017, doi: 10.1016/j.enconman.2017.02.070.
- [28] J. Xiao, T. Yang, P. Li, P. Zhai, and Q. Zhang, “Thermal design and management for performance optimization of solar thermoelectric generator,” *Applied Energy*, vol. 93, pp. 33–38, 2012, doi: 10.1016/j.apenergy.2011.06.006.
- [29] S. Shittu, G. Li, X. Zhao, and X. Ma, “Series of detail comparison and optimization of thermoelectric element geometry considering the PV effect,” *Renewable Energy*, vol. 130, pp. 930–942, Jan. 2019, doi: 10.1016/j.renene.2018.07.002.
- [30] G. Li, S. Shittu, X. Ma, and X. Zhao, “Comparative analysis of thermoelectric elements optimum geometry between photovoltaic-thermoelectric and solar thermoelectric,” *Energy*, vol. 171, pp. 599–610, Mar. 2019, doi: 10.1016/j.energy.2019.01.057.
- [31] G. Li, X. Zhao, Y. Jin, X. Chen, J. Ji, and S. Shittu, “Performance Analysis and Discussion on the Thermoelectric Element Footprint for PV–TE Maximum Power Generation,” *Journal of Electronic Materials*, vol. 47, no. 9, pp. 5344–5351, Sep. 2018, doi: 10.1007/s11664-018-6421-4.
- [32] G. J. Snyder, “Application of the compatibility factor to the design of segmented and cascaded thermoelectric generators,” *Applied Physics Letters*, vol. 84, no. 13, pp. 2436–2438, Mar. 2004, doi: 10.1063/1.1689396.
- [33] S. Shittu, G. Li, X. Zhao, and X. Ma, “Thermoelectric generator performance enhancement by the application of pulsed heat power,” 2019, doi: 10.11159/ffhmt19.146.
- [34] L. Chen and J. Lee, “Effect of pulsed heat power on the thermal and electrical performances of a thermoelectric generator,” *Applied Energy*, vol. 150, pp. 138–149, Jul. 2015, doi: 10.1016/j.apenergy.2015.04.009.
- [35] A. Ferrario, S. Boldrini, A. Miozzo, and M. Fabrizio, “Temperature dependent iterative model of thermoelectric generator including thermal losses in passive elements,” *Applied Thermal Engineering*, vol. 150, pp. 620–627, Mar. 2019, doi: 10.1016/j.applthermaleng.2019.01.031.
- [36] B. Abdessamad, K. Salah-Ddine, and C. E. Mohamed, “Design and Modeling of DC/ DC Boost Converter for Mobile Device Applications,” 2013.
- [37] M. H. Rashid, *Power electronics: circuits, devices, and applications*. Pearson Education India, 2009.
- [38] N. Mohan, T. M. Undeland, and W. P. Robbins, *Power electronics: converters, applications, and design*. John Wiley & sons, 2003.
- [39] Thejel, R. H., Ramzy S. Ali, and Elaf J. Majeed. “Novel Synthesis Methodology for Controlling Zero – Current Zero-Voltage Transition DC/DC Boost Converter.”, *Basrah Journal for Engineering Science* 6, no. 1, 2006.